Design of a Micro-Recoverable Fuze with Inertial Safety and Arming Device Under Low Overload Conditions

ShuangJie Liu*, Xudong Liu**, Nan Li***, Dawang Ma****, Lanjie Niu***** and Fuhong Chen******

Keywords：Safety and Arming Device; Recoverable; Low overload; Helical angle

ABSTRACT

Addressing the miniaturization and intelligence challenges of traditional Safety and Arming Devices (SAD), this study introduces a micro-recoverable inertial SAD capable under low overload. It integrates an inertial mass, gear set, and actuator, optimizing structure while ensuring security, reliability, and restorable safety states. Through modeling and validation, the optimal helical angle α range of 36°-53° ensures reliable unlocking and prevents self-locking. The SAD achieves a 1:3 efficient displacement and instantly returns to a safe state. Timed locking of the flameproof plate by the actuator ensures stable missile status during transitions and enhances economy & recyclability.

INTRODUCTION

A fuze is a system that utilizes target environmental information and instruction data to control the timely explosion of munitions. [1,2] It primarily comprises target detection and recognition systems, a firing control system, and a SAD (Safety and Arming Device).[3,4] The SAD ensures the safety of ammunition during handling and transportation by keeping the explosion sequence in an isolated state, while the firing control system remains in a safe state.[5] When the ammunition senses environmental cues such as launch and flight during operation, the fuze transitions from a safe to an armed state.[6-8]

Since the detonation energy is amplified step by step through the detonator, the boosting antent, and the main charge, the SAD with an isolated detonation channel can significantly improve the safety of the fuze.[9-12] To prevent accidental operation of the detonator in an abnormal environment, the detonation channel between the detonator and the boosting antent is designed in a partition state, which can only be converted to an alignment state for detonation energy transmission under specific conditions.[13] In the safe state, the primary explosive remains separated from the detonator. Only in the arming state, the detonation sequence will be aligned, the detonation energy will be output, and the warhead will be reliably detonated.[14,15]

The environmental forces used in the work of SAD are usually centrifugal force and inertial force.[16-18] However, for non-rotating munitions such as missiles, because they can only use inertial force of low magnitude to complete the arming action, it is necessary for the inertial mass block to produce a certain displacement in the direction of the projectile shaft.[19] Therefore, the traditional inertial SADs, such as Meander Slot Delay Mechanism, Sequential Delay Mechanism, and Dual Degree of Freedom Delay Mechanism, exhibit the structural characteristics of a long and narrow cylinder.[20] This feature limits the compact design of the fuze and makes it difficult to adapt to devices with strict requirements on the spatial structure. In addition, traditional SADs lack intelligent functions and cannot adaptively adjust security strategies according to real-time conditions.[21]

The Meander Slot SAD balances handling/ transportation safety with launch reliability in fuze systems. However, it encounters issues: reducing its size is challenging due to minimum inclination requirements that avoid friction increase and energy loss at inflection points. Lowering inclination for size reduction enhances security but risks self-locking during launch, compromising reliability. Additionally,

Paper Received August, 2024. Revised October, 2024. Accepted November, 2024. Author for Correspondence: Xu-Dong Liu.

* *Professor, School of Equipment Engineering, Shenyang Ligong University, Shenyang, Liaoning 110159, China.*

** *Graduate Student, School of Equipment Engineering, Shenyang Ligong University, Shenyang, Liaoning 110159, China.*

*** *Engineer, Liaoning Huaxing Electromechanical Co., Ltd, Jinzhou, Liaoning 121017, China.*

**** *Engineer, Anhui Dongfeng Electromechanical Technology Co., Ltd., Hefei, Anhui 231202, China.*

***** *Senior Engineer, Xi'an Institute of Electromechanical Information Technology, Xi'an, Shaanxi 710065, China.*

****** *Senior Engineer, Sichuan Aerospace System Engineering Institute, Chengdu, Sichuan 610100, China.*

the slot's positioning restricts the inertial cylinder's effective stroke length, negatively impacting displacement transmission.

Missiles and rockets are characterized by significant destructive power and high value.[22] In cases where ammunition cannot be detonated normally, such as due to target detection error, target disappearance, or abnormal firing control system, the fuze that has entered the ready-to-fire state becomes highly dangerous, very likely to cause unnecessary damage, and it also loses the possibility of being recovered.[23] This is because the general fuze SAD only has the one-way conversion function from the safety state to the arming state, and lacks the function to recover the ammunition from the arming state back to the safety state in cases of abnormal detonation.[24]

Therefore, there is an urgent need for a fuze SAD for low overload conditions. On the premise of ensuring the reliability of launch and the safety of handling and transportation, it breaks through the limitation of space size and improves space adaptability. Relying on a weak inertial force, the detonation transmission hole outputs a large displacement, enhancing its safety. Through the in-line detonation sequence, it can effectively avoid energy steering losses. Furthermore, it also enables the restoration of the safety state.

WORKING PRINCIPLE

Figure 1 shows the overall structure of the SAD, which is mainly composed of an inertia block, gear set, actuator, micro spring, and shell. The specific size can be altered based on the available space, and a MEMS structure can also be implemented if cost permits.

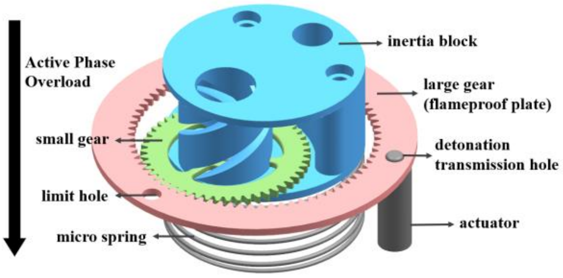

Fig 1. Structure of SAD

In the safe state, the micro-spring is in a pre-compression state, which can eliminate the influence caused by the sloshing of the inertia block. The actuator penetrates into the detonation transmission hole and locks the large gear (flameproof plate) to ensure that the SAD is not accidentally armed in cases such as handling, transportation and inadvertently dropped.

When the missile is launched, the actuator releases the restraint on the gear set upon receiving the command signal. Under the overload in the active segment, the inertia block overcomes the resistance of the spring and begins to move downward. Simultaneously, utilizing the characteristics of the helical pair to convert linear motion into rotational motion, it drives the small gear to rotate, further driving the large gear to rotate. Due to the low overload conditions of the SAD, the effect of inertia force is very limited, so a gear set with a transmission ratio of 2/3 is selected to amplify the displacement. When the small gear rotates 180°, the flameproof plate rotates 120°, aligning the detonation sequence, resulting in the SAD entering the armed state. At this point, the actuator moves, extending into the limit hole, once again completing the locking of the SAD in the armed state.

The function of restoring a fuze from the armed state to a safe state is a necessary requirement to ensure the safety of SAD. When the fuze receives the command to abort the attack, the actuator once again releases the lock on the gear set. Under the resistance of the spring, the inertia block moves upward, driving the gear set to rotate back, restoring it to the safe state, thereby preventing the missile in the 'out-of-control' state from causing unnecessary harm to unrelated objects.

THEORETICAL MODELING

As all components are affected by the overload, the gear set, when subjected to overload and pressure from the inertia block, is firmly pressed against the shell, generating huge frictional force. According to the principle of helical self-locking, when the helix angle is less than the angle of friction, the frictional resistance of the helical pair is sufficient to counteract the driving force generated by external forces, resulting in self-locking of the SAD. Mechanical analysis of the small gear is conducted, as shown in Figure 2.

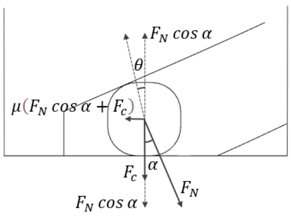

Fig 2. Force analysis

helix angle of the helical slot (α):

$$\alpha = tan^{-1}\left(\frac{h}{\pi d}\right) \tag{1}$$

In the equation, h represents the pitch of the helix, and d represents the diameter of the helix.

According to tribology principles, the friction angle of the helical pair (θ):

$$\theta = tan^{-1}\frac{\mu(F_N \cos\alpha + F_c)}{F_N \cos\alpha} \tag{2}$$

In the equation, μ represents the friction coefficient, F_c represents the inertial force acting on the gear set, and F_N represents the pressure exerted by the inertia block on the spoke of the pinion.

Analysis of self-locking condition

From equation (2), it can be observed that as the helix angle of the helical slot increases, the frictional force decreases. However, simultaneously, the normal reaction force also decreases, leading to further variations in the friction angle. The magnitude of the helix angle has a critical impact on the dynamic behavior of the SAD, determining whether the SAD can reliably be armed. To thoroughly observe this influencing mechanism and optimize its performance, the mass of the inertia block is denoted as m_l, and the mass of the gear set is denoted as m_c. k represents the stiffness coefficient of the micro-spring, and x represents the elastic deformation of the micro-spring. A mathematical model of the relationship between the helix angle (α) and the friction angle (θ) is established. Through this model, the behavior of the SAD with different helix angles can be predicted and controlled, ensuring its safety and reliability.

$$\theta = tan^{-1}\frac{\mu(m_l - kx/20g + m_c/\cos^2\alpha)}{m_l - kx/20g} \quad (3)$$

Analysis of the mathematical model reveals a positive correlation between the friction angle and the friction coefficient (μ). Self-locking phenomena typically occur at the critical state where the SAD is about to move but has not yet done so, when the friction coefficient μ is taken as the coefficient of static friction, which is usually 0.3. Additionally, in this state, only the preload of the spring resistance is considered. Based on these key parameters, a curve representing the relationship between the friction angle and the helix angle is plotted, as shown in Figure 3(a).

As the SAD transitions from static to dynamic state, the friction coefficient changes from 0.3 under static friction to 0.15 under dynamic friction. Compared to the static friction coefficient, the friction angle under dynamic friction will significantly decrease. However, the resistance of the spring increases gradually with the descent of the inertia block, leading to an increase in the friction angle. as shown in Figure 3(b).

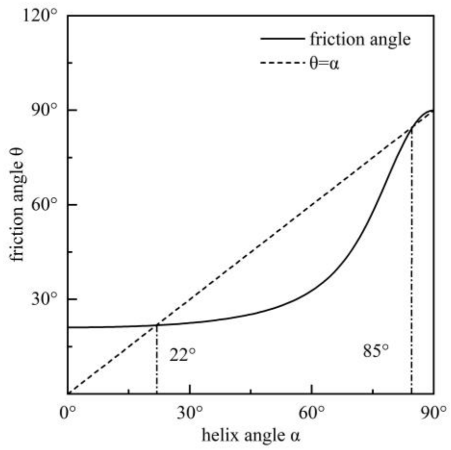

Fig. 3(a). The change of friction angle in static friction state

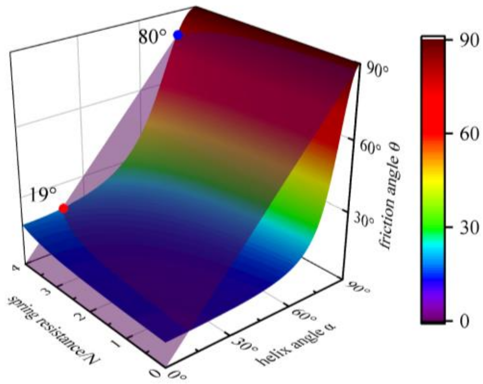

Fig. 3(b). The change of friction angle in dynamic friction state

From Figure 3(a), it can be observed that the friction angle increases with the increasing helix angle. When the helix angle (α) is less than 22°, the inertia block presses the small gear tightly against the shell, resulting in huge frictional force and causing self-locking of the SAD. When the helix angle (α) is between 22° and 85°, with the increase in the helix angle, the friction angle shows an increasing trend. When the helix angle (α) is greater than 85°, due to the friction force generated between the gear set and the shell by the inertia force being fixed, but the normal reaction force of the pressure exerted by the inertia block on the small gear approaches zero, the helical pair is in a self-locking state. When the helix angle (α) is approximately 90°, the helical slot takes a straight slot form, and the inertia block no longer contacts the small gear during the descent process, resulting in SAD failure

From Figure 3(b), it can be observed that in the dynamic state, the SAD is capable of reliably armed when the helix angle (α) is greater than 19° and less than 80°. The friction angle increases with the increasing resistance of the spring, but this increase is relatively limited. Even when the spring is compressed to its tightest, the self-locking angle is only 19°, which is less than the 22° observed under static friction. Therefore, in studying the phenomenon of self-locking, it is sufficient to consider only its static friction state

Kinematics Model

When the inertia block descends under the action of inertial force until it comes into contact with the spoke section of the pinion, the horizontal component of the resulting pressure provides the driving torque for the gear set. The gear set rotates to overcome the forces acting between them, thereby executing the arming action. For the small gear with radius r, moment of inertia I_1, and angular velocity ω_1, subjected to a force F_g from the large gear, the motion equation can be expressed as:

$$\frac{(F_l - F_R)\sin 2\alpha - 2F_g}{2} r = I_1 \frac{d\omega_1}{dt} \quad (4)$$

$$I_1 = \frac{m_1(r_1{}^2 + r_2{}^2)}{2} \quad (5)$$

For the large gear with radius R, moment of inertia I_2, and angular velocity ω_2, subjected to a force F_g from the small gear, the motion equation can be expressed as:

$$F_g R = I_2 \frac{d\omega_2}{dt} \quad (6)$$

$$I_2 = \frac{m_2\left(R_1{}^2 + R_2{}^2\right)}{2} \quad (7)$$

In addition, due to the meshing relationship between gears, the linear velocities at the meshing points must be equal, satisfying:

$$\omega_1 r = \omega_2 R \quad (8)$$

$$\frac{d\omega_1}{dt} r = \frac{d\omega_2}{dt} R \quad (9)$$

By simultaneously solving equations (4) through (9) and deriving the expression for the angular acceleration ($d_{\omega 2}/d_t$) of the detonation transmission hole under the influence of inertial forces.

$$\frac{d\omega_2}{dt} = \frac{Rr(F_l - F_R)\sin 2\alpha}{3I_1 R + 2I_2 r} \quad (10)$$

From equation (10), it is evident that the angular acceleration during the rotation of the flameproof plate is primarily influenced by inertial forces and spring resistance. As the inertia block descends, the micro-springs gradually compress, leading to a decreasing trend in the angular acceleration of the flameproof plate rotation.

Performing a second integration on equation (11) yields the relationship between the output angle (θ_2) of the detonation transmission hole and the time (t):

$$\theta_2 = \iint \frac{Rr(F_l - F_R)\sin 2\alpha}{3I_1 R + 2I_2 r} dtdt \quad (11)$$

SIMULATION

Self-locking condition simulation

Based on mathematical model analysis, the magnitude of the helical angle of the inertia block has a decisive impact on whether the SAD can be reliably armed. With the premise of ensuring that the SAD can be reliably armed, the value of the helical angle is defined not to be less than 22°. To verify the accuracy of the mathematical model, dynamic simulation verification of the SAD within the range of helical angles from 15° to 30° is conducted to study its motion characteristics.

In the ADAMS simulation software, acceleration overload ranging from 16g to 24g was applied to SAD with helical angles ranging from 15° to 30°.

To visually demonstrate the critical point of the helica angle when the SAD can reliably armed, simulation results ranging from 21° to 26° were selected for analysis, as shown in the Figures 4-5.

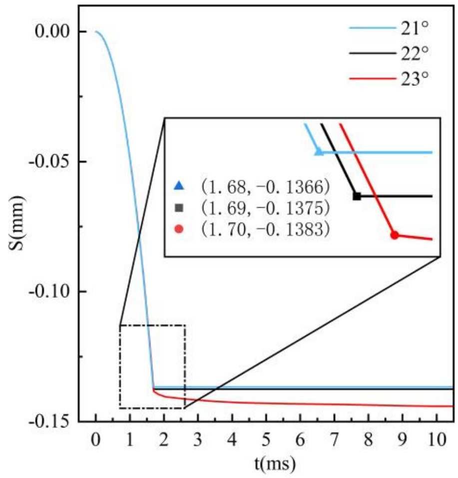

Fig. 4. The motion profile of the inertia block with 21°-23° helical slots

Through analysis of the Figure 4, it is observed that within the range of 21° to 23°, the inertia block exhibits accelerated motion during the descent initial phase due to structural clearance with the small gear. Subsequently, at approximately 1.7ms, it comes into contact with the spoke of the small gear, resulting in huge frictional force.

Among these, the inertial block with a helix angle of 23° exhibits traceable persistent sliding after undergoing a rapid stop. However, within the observation period of 100ms, its displacement is less than 1mm; therefore, it is still considered to be in a self-locking state. This phenomenon of traceable persistent sliding is attributed to the helical angle being at a critical value, placing the motion state of the inertia block at the boundary between stability and instability.

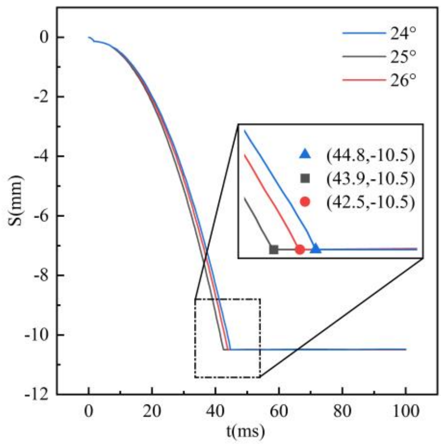

Fig. 5. The motion profile of the inertia block with 24°-26° helical slots

In contrast, the SAD within the range of 24° to 26° exhibits different motion characteristics. The inertia block descends with a certain acceleration and comes into contact with the spoke of the small gear at approximately 1.7ms, resulting in a rapid decrease in velocity. Subsequently, the inertia block descends again with an accelerating trend, while the gear set begins to rotate. At around 40ms, the inertia block reaches the bottom with a displacement of 10.5mm, and the detonation transmission hole rotates 120° with a displacement of 30.6mm, achieving alignment of the detonation sequence.

In summary, the theoretical analysis, supported by Figs. 3(a) and 3(b), indicates a helix angle range of 22° to 85° under static friction conditions and 19° to 80° under dynamic friction conditions. The intersection of these ranges results in a composite theoretical range of 22° to 80°. Further validating the theoretical findings, simulation results reveal a slightly narrower but overlapping range of 24° to 80° within which the SAD can be reliably armed. When compared to the mathematical model, the simulation results show an error of approximately 8%, which is considered relatively acceptable given the objective of exploring the optimal range of design parameters. This confirms the accuracy and effectiveness of the mathematical model.

To further enhance the reliability of the SAD's arming mechanism, a reliability coefficient of 1.5 is introduced. By applying this coefficient, the optimal range of helical angles is refined to $36° < \alpha < 53°$.

Kinematics Simulation

The micro-spring plays a role in supporting the inertial block and providing restoring force for the SAD to revert from the armed state to the safe state. Its stiffness coefficient is set at 0.3 N/mm. To eliminate the impact caused by the swaying of the inertial block and ensure the safety during the handling and transportation, the spring requires a certain preload, equivalent to a preload force of 0.5N.

Active Phase Overload of 50ms duration was applied to the SAD. The simulation results are illustrated in Figures 6 to 7. Among them, Figure 6 represent the displacement and velocity changes of the inertia block.

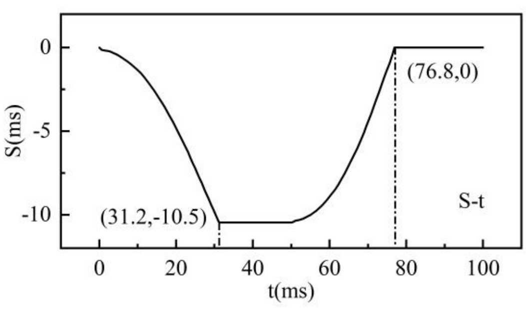

Fig. 6(a). Displacement of the inertia block.

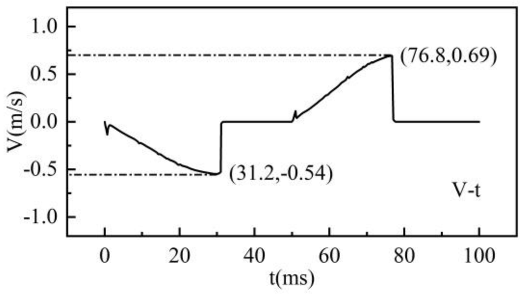

Fig. 6(b). Velocity changes of the inertia block.

From Figure 6, it can be observed that in the safe state, there exists a structural gap between the inertia block and the small gear, leading to no contact constraint between them, resulting in the inertia block exhibiting an accelerated motion. Upon contact with the small gear, the velocity of the inertia block rapidly decreases. Subsequently, the inertia block overcomes the spring resistance to move downward, simultaneously driving the gear set to rotate, again displaying an accelerated motion state, reaching its maximum velocity of 0.54m/s within 31.2ms. As the spring resistance increases to its maximum, there is a minor decrease in the velocity of the inertia block after reaching its peak. At 31.2 ms, the inertial block collides with the shell and its velocity rapidly drops to 0 m/s. At this point, the detonation transmission hole is aligned and remains so until the overload ends, with a stroke of 10.5 mm.

At 50ms, the Active Phase Overload ceases, and the restoring force provided by the micro-spring drives the inertia block to ascend, while the gear set rotates back to the safe state. Similar to the arming process, due to the structural gap, at the beginning of the restoration process, the velocity increases before decreasing. Subsequently, the inertia block ascends in an accelerated state, reaching its maximum velocity of 0.69m/s at 76.8ms. Upon contact with the shell, the velocity of all components reduces to 0m/s, and the SAD returns to the safe state. Figure 7 represent the curves of the rotation angle and angular velocity of the flameproof plate over time.

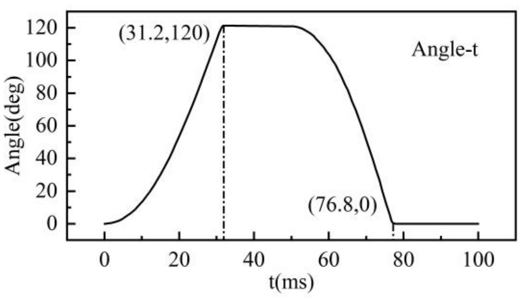

Fig. 7(a). Rotation angle of the flameproof plate over time

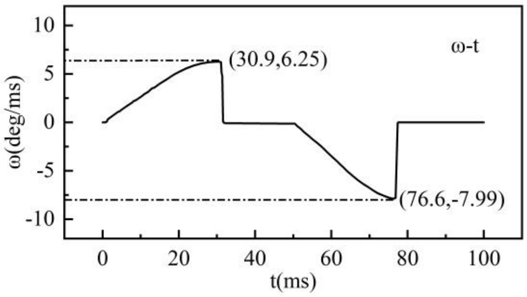

Fig. 7(b). Angular velocity of the flameproof plate over time

Similarly, from Figure 7, the collision dynamics between the inertia block and the small gear, as well as the accelerated motion process of various parts, can be observed. At 31.2ms, the detonation transmission hole rotates counterclockwise by 120° with a stroke of 30.6mm. At 76.8ms, the flameproof plate returns to the safe state. With an input of 10.5mm by the inertia block, and an output of 30.6mm by the detonation transmission hole, an approximate 1:3 displacement output rate is achieved.

The dynamic nature of the battlefield environment demands missiles to accurately hit targets in various conditions, including both active and passive stages. During the passive stage, although the Active Phase Overload ceases, the flameproof plate needs to remain in the armed position. Therefore, relying on inertial forces as the triggering mechanism for transitioning between the safe and arm states has limitations.

To overcome this limitation, this paper proposes a recoverable SAD that drives the actuator to cooperate with the limit hole through sequential power supply. When the SAD completes the arming, the actuator will sustain locking the flameproof plate to ensure its stable armed state. Only after receiving the attack cancellation signal, will the actuator release the lock on the flameproof plate, which will then automatically return to a safe state through a micro-spring, thus ensuring the safety and reliability of the SAD.

EXPERIMENT AND RESULTS

To thoroughly investigate the performance of the SAD under prolonged Active Phase Overload, a centrifuge was utilized to simulate the Active Phase Overload. Experimental validation was conducted on the SAD to ensure its reliable armed within the working range.

In the experimental setup, the distance between the centrifuge rotor axis and the SAD was set at 0.05m. To ensure that the SAD experienced the desired overload, the rotational speed of the centrifuge was calculated and set to different values to simulate varying Active Phase Overload. The SAD was mounted in a designed fixture and bolted to the centrifuge to ensure stability during the testing process, as illustrated in the Figure 8.

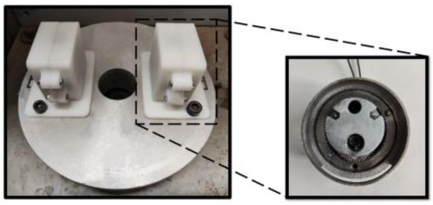

Fig 8. Centrifugal turntable after fixture fixed

Due to the non-visibility of the internal structure of the SAD after encapsulation, this study employed the method of applying a propanol mixture (a white viscous liquid) onto the base of the SAD. By observing the changes in the state of the mixture, an indirect assessment of the internal working condition of the SAD was achieved, as illustrated in the Figure 9.

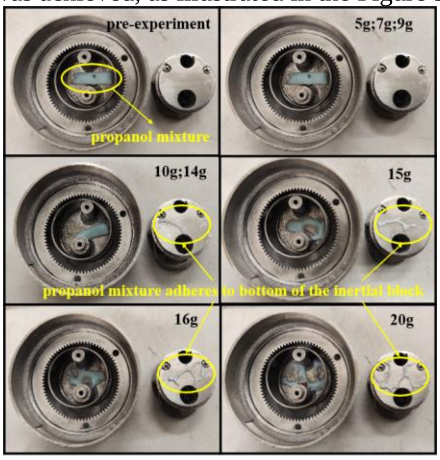

Fig. 9. Experimental result

Under a 20g overload condition, the SAD successfully completed the arming action. It was observed that the inertial block came into contact with the shell, and the propanol mixture adhered to the bottom of the inertial block. Additionally, the detonation sequence was in an aligned state, indicating that the SAD had entered the armed state. After the centrifuge rotor stopped rotating, the inertial block rose under the action of the micro-spring, and the SAD returned to a safe state. The experiments were repeated five times, and the results were as follows: the propanol mixture adhered to the bottom of the inertial block and the SAD returned to a safe state.

To comprehensively evaluate the performance of the SAD, this study also conducted tests under different overload conditions, including 5g, 7g, 9g, 10g, 14g, 15g, and 16g.

Under overload conditions of 5g, 7g, and 9g, through observation, no changes were found in the propanol mixture, indicating that the inertial block inside the SAD did not come into contact with the shell, and the detonation sequence was not aligned. Therefore, the SAD did not complete the arming.

Under 10g and 14g overloads, although there was some contact between the inertial block and the propanol mixture, no significant compression phenomenon was observed. This indicates that the inertial block did not directly contact the shell, and the detonation sequence was not aligned. Hence, the SAD also failed to complete the armed.

Under 15g and 16g overloads, the propanol mixture was significantly compressed, indicating that the inertial block had descended to and contacted the shell. Within the overload range of 15g to 16g, the SAD successfully completed the arming.

To visually demonstrate the performance of the SAD under different overload conditions and accurately determine the threshold of the Active Phase Overload, an analysis of the experimental results was conducted using a median scatter plot, as shown in the Figure 10. In the plot, each scatter point represents a specific overload condition, and its position visually reflects the working state of the SAD under that condition.

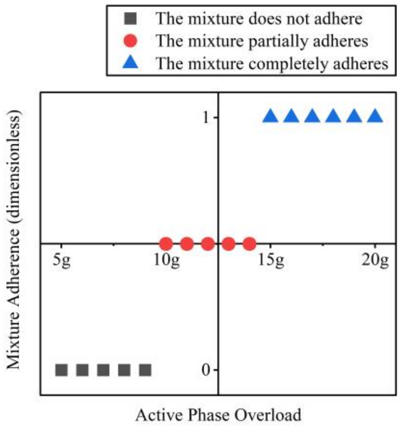

Fig. 10. The experimental results of the SAD under 5g to 20g overload conditions

Based on the aforementioned experimental results, this study concludes that when the SAD is subjected to an overload of not less than 15g, it can reliably and quickly arm, and rapidly return to a safe state after the overload disappears. This conclusion provides strong theoretical support for the application of the SAD in complex battlefield environments.

CONCLUSIONS

This article proposes a miniaturized recoverable inertial SAD suitable for low-overload conditions, which primarily consists of an inertial block, gear set, micro-spring, and actuator. Addressing the challenges of miniaturizing traditional SADs, this SAD breaks through spatial size limitations and improves compatibility while ensuring safety during handling, transportation, and accidental drops, as well as reliability during ammunition launch. Considering the influence of friction angle on the reliability of the arming, mathematical modeling and dynamic simulation analyses were conducted. It was found that when the helix angle (α) is within the range of 36°-53°, the SAD can reliably arm, avoiding self-locking phenomena. The SAD can achieve a 1:3 displacement output within 31.2 ms, enhancing safety and possessing the capability to rapidly restore to a safe state. Furthermore, the actuator will securely lock the flameproof plate to ensure its stable arming state, and can rapidly return to a safe state upon receiving an attack cancellation signal, reducing potential damage and improving economy and recyclability.

ACKNOWLEDGMENT

The Author(s) declare(s) that there is no conflict of interest

This research was supported by the following two projects:

Science and Technology on Electromechanical Dy namic Control Laboratory (Project No.: 61426010 22301)

Guangxuan Program Funding Project of Shenyang Ligong University (Project No.: LJKMZ20220601)

REFERENCES

DeKoker, J.G., “In-line fuze concept for antiarmor tactical warheads,” US Patent No. 4,421,030 (1983).

Morris, C.J., Zakar, E., Mary, B., Shaffer, E., Amirtharaj, P., and Dubey, M., “Modeling Microfabricated Multipoint Fuze Initiators Part 1: Pre-Melting Behavior,” Defense Technical Information Center, Fort Belvoir, VA (2008).

Li, H. and Zhang, X., “Three-dimensional coordinates test method with uncertain projectile proximity explosion position based on dynamic seven photoelectric detection screen,” Defence Technology, Vol. 18, pp. 1643–1652 (2022).

Jeong, J., Eom, J., Lee, S.S., Lim, D.W., Jang, Y.I., Seo, K.W., Choi, S.S., Lee, C.J., and Oh, J.S., “Miniature mechanical safety and arming device with runaway escapement arming delay mechanism for artillery fuze,” Sensors and Actuators A: Physical, Vol. 279, pp. 518–524 (2018).

Fang, K., Hu, T., Jiang, X., and Zhao, Y., “Safety and Arming Device With MEMS Based Encryption System Driven by Electrothermal Actuator,” presented at the 2020 Symposium on Design, Test, Integration & Packaging of MEMS and MOEMS (DTIP), IEEE, Lyon, France, pp. 1–5 (2020b).

Wang, S., Hao, Y., Zhang, D., and Yang, F., “The comprehensive analysis of MEMS-based fuze safety and arming device,” Journal of Detection & Control, Vol. 28, pp. 55–58 (2006).

Zheng, J., Li, Y., Hu, M., Wen, J., Wang, J., and Kan, J., "Feasibility study of a miniaturized magnetorheological grease timing trigger as safety and arming device for spinning projectile," Smart Materials and Structures, Vol. 27, p. 115030 (2018).

Gao, J., Zhao, Y., Jiang, Z., and Shang, H., "Full Silicon-based Detonation System Embedded with Micro Safety and Arming Devices," presented at the International Symposium on Test and Measurement (ISTM/2005), Dalian, China, pp. 8472–8475 (2005).

Fang, K., Hu, T., Jiang, X., and Zhao, Y., "Research on a MEMS based encrypted rotary safety and arming device," Sensors and Actuators A: Physical, Vol. 301, p. 111781 (2020a).

Xi, Z., Nie, W., and Li, Q., "A MEMS Interrupter Mechanism for Fuze Safety & Arming Device," presented at the Third International Conference on Mechanical Engineering and Mechanics, Beijing, China, pp. 51–57 (2009).

Xi, Z., Cheng, X., and Li, Z., "The Design of Setback-pin for Safety and Arming Device Based on MEMS Fuze," presented at the 4th International Conference on Mechanical Engineering and Mechanics, Suzhou, China, pp. 748–750 (2011).

Nie, W. R., Z. W. Xi, and Q. L. Li., "Process-simulation and Static Characteristic Simulation Analysis of MEMS-based Safety and Arming Device," Journal of Nanjing University of Science & Technology, Vol. 34, No. 2, pp. 166–169 (2010).

Tang, Y.J. and Wang, J., "Study of Magneto-Rheological Fluid Safe and Arming Device," Journal of Iron and Steel Research (International), Vol. 19, pp. 643–645 (2012).

Ni, Z., Liu, Y., Xie, J., Liao, Y., and Dai, J., "Investigation on the Design Method and Failure Mechanism of Silicon-Based MEMS Setback Arming Device," in: Tan, J. (Ed.), Advances in Mechanical Design, Mechanisms and Machine Science, Springer Nature Singapore, Singapore, pp. 2357–2374 (2022).

Lei, S., Cao, Y., Nie, W., Xi, Z., Yao, J., Zhu, H., Lu, H., "Research on Mechanical Responses of a Novel Inertially Driven MEMS Safety and Arming Device Under Dual-Environment Inertial Loads," IEEE Sensors Journal, Vol. 22, No. 8, pp. 7645–7655 (2022).

Han, Q., Wu, X., Yang, J., Chen, X., Zhang, J., Chao, W., and Guo, H., "Optimization and simulation of MEMS safety and arming device for the fuze," presented at the 2019 International Conference on Sensing, Diagnostics, Prognostics, and Control (SDPC), IEEE, Beijing, China, pp. 335–338 (2019).

Wang, D., Lou, W., Feng, Y., Zhang, X., "Design of High-Reliability Micro Safety and Arming Devices for a Small Caliber Projectile," Micromachines, Vol. 8, No. 8, pp. 234 (2017).

Sun, D., Tang, Y., Wang, J., Wang, X., "Design of an H-shaped linear piezoelectric motor for safety and arming device," Sensors and Actuators A: Physical, Vol. 303, pp. 111687 (2020).

Westphal, G., Kienzler, F., and Höni, H., "Safety and arming device for a spinning projectile fuze," US Patent No. 7,367,268 B2 (2008).

Titus, J.D. and Hall, P.E., "Electro-explosive safety and arming device," US Patent No. 4,691,634 (1987).

Rehan, M., Mansoor, M., "Application of MEMS in safety and arming devices: an overview," Microsystem Technologies, Vol. 27, No. 10, pp. 3599–3610 (2021).

Tu, H., Lou, W., Sun, Z., Qian, Y., "Structural reliability simulation for the latching mechanism in MEMS-based Safety and Arming device," Advances in Engineering Software, Vol. 108, pp. 48–56 (2017).

Wang, F. F., Lou, W. Z., Liu, F. Y., Wang, D. K., Lu, J., Wu, J., Guo, X. H., Zhang, Z., "The Buckling Simulation of Planar W-Form Micro-Spring in MEMS Safety and Arming Device," Key Engineering Materials, Vol. 645–646, pp. 796–799 (2015).

Ma, W. R., He, G., "Effect of Strain Rate on the Simulation of MEMS Safety and Arming Device," Key Engineering Materials, Vol. 609–610, pp. 849–855 (2014).

NOMENCLATURE AND UNIT

α helical angle, deg

h The lead of the helical line, m

d The diameter of the helical line, m

θ The angle of friction, deg

μ coefficient of friction, dimensionless

F_N the pressure exerted by the inertia block on the spoke of the pinion, N

x the elastic deformation of the micro-spring, m

F_c the inertial force acting on the gear set, N

m_l the mass of the inertia block, kg

g Gravitational Acceleration, 9.8m/s

m_c the mass of the gear set, kg

τ the active phase, m/s²

F_l Inertia force of inertia block, N

F_R spring resistance, N

m The mass of the inertial block, kg

a Acceleration of inertial block, m/s²

F_g Interaction force between gear set, N

r Radius of small gear, m

I_1 Moment of inertia of small gear, kg·m²

ω_1 Angular velocity of small gear, rad/s

t Time, s

m_1 The quality of small gear, kg

r_1 The inner diameter of small gear, m

r_2 The outer diameter of small gear, m

R Radius of large gear, m

I_2 Moment of inertia of large gear, kg·m²

ω_2 Angular velocity of large gear, deg/ms

m_2 The quality of large gear, kg

R_1 The inner diameter of large gear, m

R_2 The outer diameter of large gear, m